frontiers

Supplementary Material of

North Atlantic Western Boundary Currents are intense dissolved organic carbon streams

Marcos Fontela[1,2*], Fiz F. Pérez[1], Herlé Mercier[3], Pascale Lherminier[3]

[1] Instituto de Investigaciones Marinas, IIM-CSIC, 36208 Vigo, Spain.
[2] Centre of Marine Sciences (CCMAR), University of Algarve, 8005-139 Faro, Portugal.
[3] University of Brest, Laboratoire d'Océanographie Physique et Spatiale, UMR 6523 CNRS-IFREMER-IRD-University of Brest, Plouzané, France.

*** Correspondence:**
Corresponding Author
fiz.perez@iim.csic.es

This Supplementary Material includes, by order of appearance in the main text, the following information:

- **Table S1**. DOC water mass definitions by eOMP analysis.
- **Table S2.** Transports at the Greenland-Scotland (G-S) Ridge.
- **Table S3.** Transports at 24.5ºN.
- **Figure S1.** Longitudinal distribution of intermediate waters [DOC].
- **Figure S2**. Measured versus modelled transports: an insight into its difference

Table S1. DOC water mass definitions by eOMP analysis

The methodology of the modelled transports is based in an extended Optimum Multiparameter (eOMP) analysis that solves the water mass structure of the OVIDE section (García-Ibáñez et al., 2015). OMP analyses are based on the premise that the water mass fractions that constitute a sample can be reproduced by an appropriate mixture of some well-known Source Water Types (SWT), which are characterized by water mass tracers like temperature (Θ) and salinity (S). OMP analyses obtain the water mass fractions (X_i) by solving a system of linear equations describing the measured water mass properties in terms of mixing of SWT. Each equation of the system is weighted in relation to the accuracy of the measured property. The main difference between classical (cOMP, Tomczak, 1981) and extended OMP analyses is that the latter includes both conservative and non-conservative variables. We constrained the OMP analysis to the water samples with pressure ≥100 dbar to avoid the non-conservative behavior of Θ and S in the surface layer due to air-sea interactions after the last maximum of winter convection (García-Ibáñez et al., 2015). The OMP has been successfully used in previous studies with similar needs for solving water mass mixing (Pardo et al., 2012; Fontela et al., 2016; de la Paz et al., 2017). The system of equations in the first step of the eOMP is similar to that of the cOMP and based on conservative variables. It is as follows:

$$\sum_{i=1}^{n} X_i * \theta_i^{SWT} = \theta^{sample} + R_\theta$$

$$\sum_{i=1}^{n} X_i * S_i^{SWT} = S^{sample} + R_S$$

$$\sum_{i=1}^{n} X_i * SiO_{2i}^{SWT} = SiO_2^{sample} + R_{SiO_2}$$

$$\sum_{i=1}^{n} X_i * NO_i^{SWT} = NO^{sample} + R_{NO}$$

$$\sum_{i=1}^{n} X_i * PO_i^{SWT} = PO^{sample} + R_{PO}$$

$$\sum_{i=1}^{n} X_i = 1 + R_{mass}$$

where *Rp* is the residual of each measured property p^{sample} (Θ, S, SiO_2, NO=10.5*NO_3+O_2 and PO=175*PO_4+O_2, Broecker, 1974; Takahashi et al., 1985; Anderson and Sarmiento, 1994) that the OMP tries to minimize and P_i^{SWT} is the property of each SWT_i. The last equation accounts for the mass conservation. The cOMP analysis is solved for different mixing figures, which are groups of SWTs that are susceptible to mix together, and are set considering the vertical characteristics and/or dynamics of the SWTs in the region of study. The most appropriate mixing figure is selected as the mixing figure that gives to the water sample the lowest residuals.

Using the same set-up as the cOMP, an eOMP analysis is solved also considering non-conservative variables (SiO_2, NO_3, PO_4 and O_2). A new unknown has to be considered, ΔO, which refers to changes in O_2 due to the remineralization of the organic matter.

$$\sum_{i=1}^{n} X_i * \theta_i^{SWT} = \theta^{sample} + R_\theta$$

$$\sum_{i=1}^{n} X_i * S_i^{SWT} = S^{sample} + R_S$$

$$\sum_{i=1}^{n} X_i * SiO_{2i}^{SWT} + \Delta O / r_{Si} = SiO_2^{sample} + R_{SiO_2}$$

$$\sum_{i=1}^{n} X_i * O_{2\,i}^{0\,SWT} - \Delta O = O_2^{sample} + R_{O_2}$$

$$\sum_{i=1}^{n} X_i * NO_{3\,i}^{0\,SWT} + \Delta O / r_N = NO_3^{sample} + R_{NO_3}$$

$$\sum_{i=1}^{n} X_i * PO_{4\,i}^{0\,SWT} + \Delta O / r_P = PO_4^{sample} + R_{PO_4}$$

$$\sum_{i=1}^{n} X_i = 1 + R_{mass}$$

where R_{SiO2} is 12, R_{NO3} is 10.5 and R_{PO4} is 175 (Takahashi et al., 1985; Anderson and Sarmiento, 1994). The cOMP analysis selects the mixing figure based on conservative water mass tracers; once the mixing figures are selected, the estimates of the X_i are given by the eOMP analysis, which takes into account the effect of the biology in the measured variables.

With the water mass structure, the [eDOC] for each SWT ($[eDOC]_i$) can be solved by an inversion of the eOMP equations (Table S1).

Table S1. Water mass eDOC characterization. Potential temperature (Θ), salinity (S) and non-refractory dissolved organic carbon (e[DOC]^{eOMP}, in µmol·kg^{-1}) of each Source Water Type* considered here with their corresponding standard deviations. Correlation coefficient (r^2) between interpolated and estimated DOC is given together with the number of analyzed DOC samples (*n* measured) and the number of samples with known water mass structure (*n* eOMP data). The standard deviations of the residuals (SDR) and the SDR/ε ratios, with ε being the DOC measurement error, are also given.

	Θ (ºC)	Salinity	e[DOC]^{eOMP} (µmol·kg^{-1})
$ENACW_{16}$	16.0±0.1	36.2±0.02	24.2±0.9
$ENACW_{12}$	12.3±0.2	35.7±0.03	14.8±0.2
MW	11.7±0.2	36.5±0.01	3.5±0.4
SAIW	6.0±0.2	34.7±0.03	11.0±0.4
$SPMW_8$	8.0±0.1	35.2±0.02	8.5±0.4
$SPMW_7$	7.1±0.1	35.2±0.01	13.2±0.4
IrSPMW	5.0±0.0	35.0±0.01	15.6±0.5
LSW	3.0±0.2	34.9±0.02	8.9±0.1
ISOW	2.6±0.1	35.0±0.00	9.0±0.3
DSOW	1.3±0.1	34.9±0.01	14.4±0.7
PIW	0.0±0.2	34.7±0.03	9.4±2.5
$NEADW_L$	2.0±0.0	34.9±0.00	1.6±0.2
n measured			581
n eOMP data			3899
r^2			0.56
SDR			3.4

* $ENACW_{16}$ and $ENACW_{12}$: East North Atlantic Central Waters; MW: Mediterranean Water; SAIW: Subarctic Intermediate Water; $SPMW_8$ and $SPMW_7$: Subpolar Mode Waters of the Iceland Basin and IrSPMW of the Irminger Basin; LSW: Labrador Sea Water; ISOW: Iceland-Scotland Overflow Water; DSOW: Denmark Strait Overflow Water; PIW: Polar Intermediate Water; and $NEADW_L$: lower North East Atlantic Deep Water.

Table S2. Transports at the Greenland-Scotland (G-S) Ridge.

The exchanges of the eastern Subpolar North Atlantic (eSPNA) with the Nordic Seas are restricted by the G-S Ridge topography. The shallow depth of the sill, around 500 m, limits the exchange of deep water with the North Atlantic. The only regions that allow relatively deep overflows are the Denmark Strait and the Faroe Bank Channel. Shallower overflows also occur across the Iceland-Faroe Ridge, a broad ridge with minimum depths of 300–500 m (deepening at the Faroese end), and the Wyville-Thomson Ridge between the Faroes and the Scotland shelf (depth ~600 m). This bathymetric restriction narrows the variability in annual circulation, so available transport estimates are robust (Østerhus et al., 2019).

The upper water masses in northward direction are the East North Atlantic Central Water (ENACW), Modified North Atlantic Central Water (MNACW) and North-Iceland Irminger Water (NIIW). The water masses in southward direction are the surface flowing Polar Intermediate Water (PIW), and the overflows Denmark Strait Overflow Water (DSOW) and Iceland-Scotland Overflow Water (ISOW). **Table S2.** Volume transports (in Sv; 1 Sv=10^6 $m^3 \cdot s^{-1}$) from Østerhus et al., (2019). Positive (negative) transports are northward (southward). Density (in $kg \cdot m^{-3}$) and [DOC] (in $\mu mol \cdot kg^{-1}$) are taken from Jeansson et al., (2011) and converted to eDOC ([eDOC]=[DOC]-[$DOC_{refractory}$], where [$DOC_{refractory}$]=40 $\mu mol \cdot kg^{-1}$).

Water mass	Volume transport (Sv)	Density ($kg \cdot m^{-3}$)	e[DOC] ($\mu mol \cdot kg^{-1}$)
ENACW	(3.3 + 0.45*) 3.75 ± 0.6	1027.3	18 ± 1.2
MNACW	3.8 ± 0.5	1027.4	18 ± 1.2
NIIW	0.9 ± 0.1	1027.6	19 ± 1.3
PIW	-2 ± 0.5	1027.4	30 ± 4.3
DSOW	-3.2 ± 0.5	1027.9	18 ± 1.9
ISOW	-2.6 ± 0.3	1028	13 ± 1.2
TOTAL	0.65		

Table S2

The ENACW transport has been modified from the original 3.3 Sv (2.7 Sv from the Faroe Scotland-inflow and 0.6 Sv from European Shelf Atlantic inflow; Østerhus et al., 2019) to 3.75 Sv. The difference, 0.45 Sv, is added to the ENACW with the purpose of maintain a net northward transport of 0.65 to ensure mass conservation in the eSPNA budget. The modification of ENACW is supported by the fact that is the most variable flux across the G-S Ridge (Østerhus et al., 2019).

Using data from the following table, we computed the transport of eDOC at the G-S Ridge with the Equation S1.

$$T_{eDOC}^{G-SR} = \sum_{i=1}^{6} T_i^{G-SR} \cdot [eDOC]_i \cdot \bar{\rho}_i \ (Equation\ S1)$$

Table S3. Transports at 24.5ºN.

We reconstructed the eDOC transports at subtropical latitudes (24.5–26.5ºN) for the RAPID period (2004–2017) based on the work of Hansell et al., (2004) and the data of the RAPID-MOC time series (Smeed et al., 2018) following the methodology of Fontela et al., (2016). The $[DOC]_{mean}$'98 available in Fontela et al., (2016) was converted to $[eDOC]_{mean}$'98 ($[eDOC]=[DOC]-[DOC_{refractory}]$, where $[DOC_{refractory}]=40$ µmol·kg^{-1}).and then combined with the average volume transport in RAPID-MOC time series (in Sv, Smeed et al., 2018). The volume transport is the mean transport between the dates 2 April 2004 and 28 February 2017. All data required for eDOC transport (kmol·s^{-1}) computations at subtropical latitudes (24.5–26.5ºN) are given in the following **Table S3**:

Layers	Volume transport (Sv)	Density (kg·m^{-3})	e[DOC]mean'98 (µmol·kg^{-1})	eDOC transport (kmol·s^{-1})	
Ekman	3.67	1030	27.9	106	239
Upper mid-ocean	-18.02		15.6	-289	
Gulf Stream	31.4		13.1	423	
Deep ocean	-17.8	1034	0.6	-10	-7
Deeper than 5000m	1.02		2.5	3	

Table S3

The RAPID/MOCHA/WBTS array is a collaborative effort supported through the UK Natural Environment Research Council (NERC) RAPID-WATCH program, the US National Science Foundation (NSF) Meridional Overturning Circulation Heat-flux Array project, and the US National Oceanographic and Atmospheric Administration (NOAA) Western Boundary Time Series project; and transports including error estimates were freely available at www.rapid.ac.uk/rapidmoc

Supplementary Figure 1. Longitudinal distribution of intermediate waters [DOC].

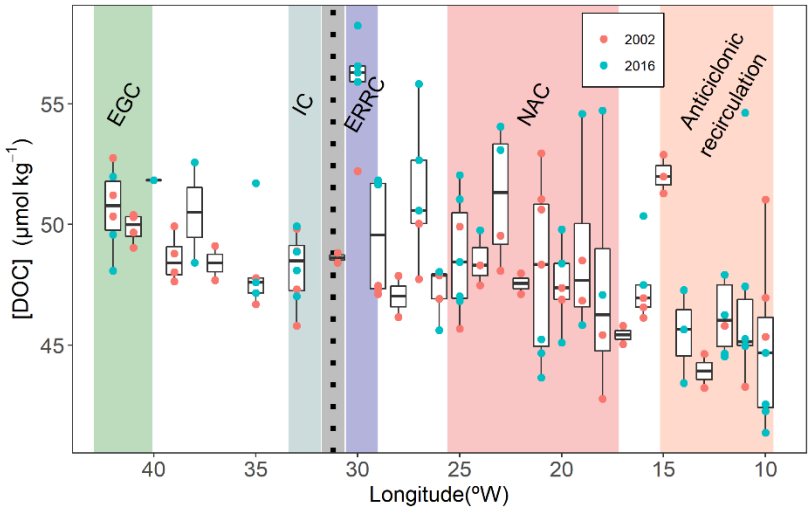

Supplementary Figure 1. Longitudinal distribution of [DOC] (in µmol·kg^{-1}) at intermediate waters (1000-2000 m). Samples are grouped by Longitude (ºW) at 1º resolution. Year 2002 (2016) samples are represented in red (blue). There is an increase in [DOC] of intermediate waters from East to West.

Supplementary Figure 2 Measured versus modelled transports: an insight into its difference

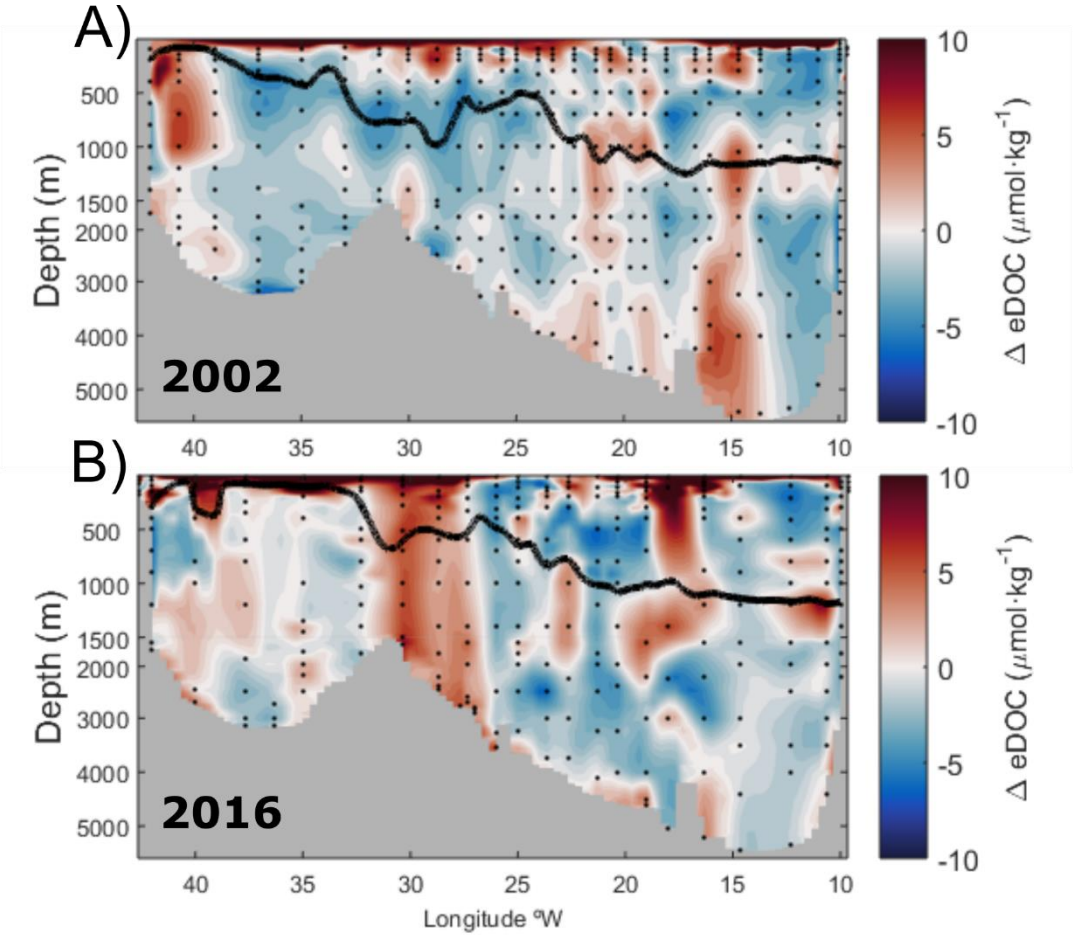

Figure 3. Vertical distribution of the anomaly of eDOC (eDOC measured minus eDOC modelled with the eOMP, in µmol·kg^{-1}) along the OVIDE A) 2002 and B) 2016 section from Greenland (left) to the Iberian Peninsula (right). Positive anomalies imply that modelled concentrations are underestimations and vice versa. Isopycnal σ_{AMOC} (black line) separates the upper and lower limbs of AMOC. Note that the depth scale is not linear. Differences between the concentrations measured and modelled (Δ[eDOC]=[eDOC]^{interp} - [eDOC]^{eOMP}) are unevenly distributed along the OVIDE section for 2002 and 2016. The median of the differences is 1.6±0.7 µmol·kg^{-1} and 2.0±0.7 µmol·kg^{-1} for the years 2002 and 2016 respectively. Besides the general agreement, some specific patterns appear: (i) in the upper layer, concentrations of eDOC are larger than predicted by the eOMP; (ii) in the western boundary currents, there is an almost full-depth vertical pattern of underestimation predicted by the eOMP. The underestimation in the East Greenland Current appears in 2002 rather than 2016 while, in contrast, east of the Reykjanes Ridge it is more clearly evident in 2016 than in 2002. In 2002, there is a vertical anomaly in the Iberian Abyssal Plain (~15ºW) related with a single-station profile already identified as unusually high with the water mass reconstruction approach (Fontela et al., 2016). We suggest that this anomaly is related to an isolated measurement bias at that specific station. Its influence on the transport is low because it is located southeast of the NAC where the net volume transport is close to zero. In 2016, the underestimation of the model reaches mid-depth (500-750 m) in the Irminger Sea at 40ºW and 2000 m between 15-20ºW. At 40°W, the deepening of the σ_{AMOC} isopycnal (Fig. 3) is coincident with a downwelling of DOC-enriched superficial waters due to eddy activity. The

anomaly at 15-20ºW could be related with the extraordinary amount of subarctic water that reached the OVIDE section from the western Subpolar North Atlantic in the summer of 2016 (Holliday et al., 2020). The eOMP that leads the $[DOC]^{eOMP}$ reconstruction does not allow Subarctic Intermediate Water (SAIW) to reach so far away from its formation region in the Labrador Sea (García-Ibáñez et al., 2015). Consequently, the neglect of the large [DOC] contribution of this water mass (Álvarez-Salgado et al., 2013; Fontela et al., 2016) resulted in an underestimation with respect to measurements.

References

Álvarez-Salgado, X. A., Nieto-Cid, M., Álvarez, M., Pérez, F. F., Morin, P., and Mercier, H. (2013). New insights on the mineralization of dissolved organic matter in central, intermediate, and deep water masses of the northeast North Atlantic. *Limnol. Oceanogr.* doi:10.4319/lo.2013.58.2.0681.

Anderson, L. A., and Sarmiento, J. L. (1994). Redfield ratios of remineralization determined by nutrient data analysis. *Global Biogeochem. Cycles* 8, 65–80. doi:10.1029/93GB03318.

Broecker, W. S. (1974). "NO", a conservative water-mass tracer. *Earth Planet. Sci. Lett.* doi:10.1016/0012-821X(74)90036-3.

de la Paz, M., García-Ibáñez, M. I., Steinfeldt, R., Ríos, A. F., and Pérez, F. F. (2017). Ventilation versus biology: What is the controlling mechanism of nitrous oxide distribution in the North Atlantic? *Global Biogeochem. Cycles*. doi:10.1002/2016GB005507.

Fontela, M., García-Ibáñez, M. I., Hansell, D. A., Mercier, H., and Pérez, F. F. (2016). Dissolved Organic Carbon in the North Atlantic Meridional Overturning Circulation. *Sci. Rep.* 6. doi:10.1038/srep26931.

García-Ibáñez, M. I., Pardo, P. C., Carracedo, L. I., Mercier, H., Lherminier, P., Ríos, A. F., et al. (2015). Structure, transports and transformations of the water masses in the Atlantic Subpolar Gyre. *Prog. Oceanogr.* doi:10.1016/j.pocean.2015.03.009.

Hansell, D. A., Ducklow, H. W., Macdonald, A. M., and Baringer, M. O. (2004). Metabolic poise in the North Atlantic Ocean diagnosed from organic matter transports. *Limnol. Oceanogr.* 49, 1084–1094. doi:10.4319/lo.2004.49.4.1084.

Holliday, N. P., Bersch, M., Berx, B., Chafik, L., Cunningham, S., Florindo-López, C., et al. (2020). Ocean circulation causes the largest freshening event for 120 years in eastern subpolar North Atlantic. *Nat. Commun.* doi:10.1038/s41467-020-14474-y.

Jeansson, E., Olsen, A., Eldevik, T., Skjelvan, I., Omar, A. M., Lauvset, S. K., et al. (2011). The Nordic Seas carbon budget: Sources, sinks, and uncertainties. *Global Biogeochem. Cycles* 25, GB4010. doi:10.1029/2010GB003961.

Østerhus, S., Woodgate, R., Valdimarsson, H., Turrell, B., De Steur, L., Quadfasel, D., et al. (2019). Arctic Mediterranean exchanges: A consistent volume budget and trends in transports from two decades of observations. *Ocean Sci.* doi:10.5194/os-15-379-2019.

Pardo, P. C., Pérez, F. F., Velo, A., and Gilcoto, M. (2012). Water masses distribution in the Southern Ocean: Improvement of an extended OMP (eOMP) analysis. *Prog. Oceanogr.*

doi:10.1016/j.pocean.2012.06.002.

Smeed, D. A., Josey, S. A., Beaulieu, C., Johns, W. E., Moat, B. I., Frajka-Williams, E., et al. (2018). The North Atlantic Ocean Is in a State of Reduced Overturning. *Geophys. Res. Lett.* doi:10.1002/2017GL076350.

Takahashi, T., Broecker, W. S., and Langer, S. (1985). Redfield ratio based on chemical data from isopycnal surfaces. *J. Geophys. Res.* 90, 6907–6924. doi:10.1029/JC090iC04p06907.

Tomczak, M. (1981). A multi-parameter extension of temperature/salinity diagram techniques for the analysis of non-isopycnal mixing. *Prog. Oceanogr.* 10, 147–171. doi:10.1016/0079-6611(81)90010-0.